Generalized Approach to NMR Analysis of Flow and Dispersion in Porous Media

Joseph D. Seymour and Paul T. Callaghan
Dept. of Physics, Massey University, Palmerston North, New Zealand

A generalized approach to the use of pulsed-gradient spin echo (PGSE) NMR methods for the measurement of flow and diffusion in porous media is presented, in which the fluid dynamics is probed over well-defined temporal and spatial domains. Various NMR techniques based on PGSE encoding are described in the context of standard theories of dispersion, with reference to Eulerian and Lagrangian coordinate frames. This array of methods provides access not only to the dispersion coefficient and the mean local velocity but also to propagators relevant to spatial and temporal correlations. Methods investigated include flow imaging, average propagator analysis, dispersion measurement, velocity exchange spectroscopy, and flow diffraction based on scattering analysis. We apply these to a study of flow and dispersion of water in a packed bed of 90.7-μm-dia. polystyrene latex spheres. Our measurements of the dependence on Peclet number of dispersion (parallel and perpendicular to the mean flow direction) are in excellent agreement with results reported in the literature. The scattering approach used here has potential for studying complex flow properties involving the interplay between hydrodynamic and structural characteristics of porous media.

Introduction

The subject of flow and transport in porous media has major interdisciplinary significance. An understanding of these phenomena underpins liquid chromatographic separation technology, packed-bed-reactor design, modeling of contaminant transport in geological media, and studies of perfusion in biological tissue, to name but a few. Transport behavior in porous media is governed by the interaction of diffusive and advective processes, in other words, the phenomenon of dispersion. Central to any understanding of dispersion is the matter of scale dependence. The effect on measured transport coefficients of interactions between the spatial and temporal scales of observation and the natural scales of the media, becomes a primary issue both in the modeling of porous media and in any comparisons between theory and experiment (Whitaker, 1986; Cushman, 1990). In this article we address these problems from the standpoint of a particular measurement technique, nuclear magnetic resonance (NMR).

NMR has proven of enormous value in the investigation of fluids in porous media. Bulk measurements of NMR signal amplitude can be used to obtain porosity values. Because of surface relaxivity effects, the analysis of NMR relaxation times can provide information about pore-surface-to-volume ratios and pore-size distributions (Davies et al., 1991). Measurements of fluid diffusivity can reveal pore tortuosity (Callaghan et al., 1991, 1992; Mitra et al., 1993), while NMR flow measurements can be used to obtain estimates of permeability.

The development of NMR imaging has led to a number of applications in which NMR parameters are mapped directly. Most obvious among these is the fluid distribution itself. In principle such an imaging experiment can provide a map of the pore space, provided that the pore size is significantly larger than the intrinsic imaging volume element (the voxel). Recently, a number of researchers have reported NMR experiments in which fluid is forced through a porous medium and a map of the fluid velocity is reconstructed (Guilfoyle et al., 1992; Chen et al., 1993; Kutsovsky et al., 1996; Mansfield and Issa, 1996), in some cases with a spatial resolution larger than the pore size and in others, where media with very coarse

Correspondence concerning this article should be addressed to P. T. Callaghan.
Present address of J. D. Seymour: The Lovelace Institutes, 2425 Ridgecrest Dr. SE, Albuquerque, NM 87108.

structure are employed, on a sufficiently fine resolution scale that the flow profile is visible within a single pore.

The use of imaging methods, while powerful in one sense, involves an inevitable "trade-off" in another. Because NMR suffers from intrinsically weak sensitivity, every "well-designed" experiment will optimize for the parameters under investigation. The ability to obtain information about structural heterogeneity via imaging comes at the price of reduced sensitivity to other parameters, and most particularly of relevance to the case of flow in porous media will be any sacrifice in the resolution available for the temporal dimension of the velocity field. It is partly for this reason that many other NMR techniques are often employed in the investigation of fluid motion, techniques that deliberately relinquish spatial resolution. As we shall show, however, another delicate factor often not appreciated explicitly by practitioners is the sense in which the sacrifice of spatial resolution can lead to the measurement of parameters that are better defined in the Lagrangian sense.

The techniques by which NMR can be used to obtain information about fluid motion are multitudinous. We shall restrict our discussion to those based on the use of magnetic-field gradients, since this set, which depends on phase-encoding methods, is characterized by the greatest precision, accuracy, and subtlety. These methods include, in addition to direct velocity imaging, average propagator analysis, time-dependent dispersion measurement, "q-space diffraction," velocity exchange spectroscopy, and frequency-domain analysis using modulated gradients.

A review of the generalized analysis of fluid motion using magnetic-field gradients has been provided recently by Callaghan and Stepišnik (1996), and we refer the reader to this article for details of the underlying NMR theory. In the present article we are concerned with the implementation of some of these analytical methods, applying a spectrum of techniques by way of illustration to a specific porous medium. This medium is chosen to exhibit characteristic dimensions that make it amenable to the widest possible range of useful strategies. We illustrate how the various methodologies can provide differing but complementary insights regarding the flow. In each case we attempt to precisely define the relevant hydrodynamic quantities to which we are sensitive, clearly indicating the time and length scales over which any averaging takes place. By this means we hope that the presentation will serve a didactic purpose, helping to draw together the various strands that underpin the NMR perspective and, hopefully, providing a framework in which the links between the methods are apparent.

The organization of the article is as follows. The first section presents a brief overview of some selected concepts from the theory of dispersion in porous media, so that these ideas can be subsequently incorporated into the discussion of the NMR methods. The second section provides details of the experimental apparatus and measurement conditions. The following sections deal successively with a different NMR methodology. In each of these the respective NMR method is described in as rigorous and clearly defined a manner as possible, illustrating the application of this method to the experimental system under investigation, namely flow in a packed column of monodisperse spheres. In each case we aim to provide a clear connection to the theory of dispersion.

Dispersion in Porous Media

The theory of dispersion in porous media has been treated using several different methodologies. An essential component of porous media modeling concerns the existence of a hierarchy of scales over which transport occurs (Cushman, 1990). A common feature of many approaches is the averaging, or coarse graining, of transport equations valid at some microscale, a device employed so as to permit derivation of macroscopic behavior. Both the asymptotic and nonasymptotic, or local and nonlocal (Koch and Brady, 1987; Brady, 1990), dispersion theories are relevant here, as NMR is capable of providing data over spatial and temporal scales relating to both regimes. We present only brief statements of some results from the theory directly used in this article. The interested reader is referred to the large number of articles, reviews, and books on the subject (Bear, 1972; Brenner, 1980; Dagan, 1989; Cushman, 1990; Quintard and Whitaker, 1993; Sahimi, 1993).

The presentation here parallels the concise discussion of Brady (1990). The asymptotic, or local (a nomenclature based on the fact that it depends only on the local mean concentration gradient (Koch and Brady, 1987)), Lagrangian dispersion tensor is defined from the method of moments (Brenner, 1980; Salles et al., 1993) and the formalism of stationary stochastic processes (Van den Broeck, 1990) as

$$\boldsymbol{D}^* = \lim_{t\to\infty} \frac{1}{2}\frac{d\boldsymbol{\sigma}^2(t)}{dt} = \mathrm{sym}\int_0^t <\boldsymbol{u}(0)\boldsymbol{u}(\tau)>\, d\tau, \quad (1)$$

where $\boldsymbol{\sigma}^2(t) = <(\boldsymbol{r}(t) - <\boldsymbol{r}(t)>)^2>$ is the positional variance; $\boldsymbol{u}$ is the fluctuation in the Lagrangian velocity field, $\boldsymbol{u} = \boldsymbol{v} - \boldsymbol{V}$; and the symmetry operator is sym $(\boldsymbol{A}) = \frac{1}{2}(\boldsymbol{A} + \boldsymbol{A}^T)$. The average velocity is defined by

$$\boldsymbol{V} \equiv \lim_{t\to\infty} \frac{d<\boldsymbol{r}(t)>}{dt} = \lim_{t\to\infty} \langle \boldsymbol{v} \rangle,$$

where $\boldsymbol{v}$ is the local instantaneous velocity. The ensemble average, $\langle\,\rangle$, is taken over the distribution of velocity fields (Koch and Brady, 1987) localized in space. Notice that the long time limit is taken with respect to the correlation time of the velocity fluctuations (Brady, 1990).

The definition of the dispersion given in Eq. 1 arises from the theory of stochastic processes (Van den Broeck, 1990) and relates directly to NMR measurements of the effect of motion on the sample magnetization, a method whose description is inherently statistical, as evidenced by the use of a density matrix formalism (Stepišnik, 1981; Callaghan and Stepišnik, 1996).

Dispersion in the preasymptotic regime and anomalous dispersion due to heterogeneity of the porous media require a nonlocal formulation (Koch and Brady, 1987; Brady, 1990; Cushman, 1990). The time step and displacement-dependent nonlocal dispersion tensor are given by (Koch and Brady, 1987; Brady, 1990)

$$\boldsymbol{D}^*(\boldsymbol{r}-\boldsymbol{r}', t-t') = \langle \boldsymbol{u}(\boldsymbol{r},t)P(\boldsymbol{r}, t \mid \boldsymbol{r}', t')\boldsymbol{u}(\boldsymbol{r}',t')\rangle, \quad (2)$$

where $P(\boldsymbol{r},t \mid \boldsymbol{r}',t')$ is the transition probability, or propagator,

of a tracer from $\boldsymbol{r}$ at t to $\boldsymbol{r}'$ at t'. The propagator is governed by the microscale advection-diffusion equation at each point in the media. The local dispersion coefficient is obtained from the nonlocal form by integrating over $\boldsymbol{r}'$ and t' in Eq. 2.

The dispersion coefficients just defined are consistent with a macroscopic transport equation of the form

$$\frac{\partial\langle c\rangle}{\partial t}+\boldsymbol{V}\cdot\nabla\langle c\rangle=\nabla\cdot(\boldsymbol{D}_E^*\cdot\nabla\langle c\rangle), \tag{3}$$

where $\langle c\rangle$ is the average concentration (or probability density) of solute; and $\boldsymbol{D}_E^*$ the Eulerian dispersion tensor, related to the Lagrangian dispersion tensor defined in Eq. 1 by $\boldsymbol{D}^*=\text{sym}\,\boldsymbol{D}_E^*$ (Koch et al., 1989). Averaged transport models akin to Eq. 3 have been derived by several methods. A common feature of these approaches is that the dispersion coefficient is dependent on the fluctuations in velocity, as in Eq. 1, through a closure problem on higher-order correlations, or moments. The form of the closure problem is identical when derived by the ensemble average technique (Koch et al., 1989), the method of moments (Brenner, 1980), and the method of homogenization (Rubinstein and Mauri, 1986), and possesses many similarities with that developed by the method of volume averaging (Quintard and Whitaker, 1993).

Finally, we note that the mechanisms that cause dispersion are often discussed in terms of three principal processes. Mechanical dispersion is due to stochastic variations in velocity introduced by advection along tortuous paths and flow bifurcations and scales with Peclet number, *Pe*. Diffusive (Taylor) dispersion (Taylor, 1953) arises from molecular diffusion across streamlines and scales as Pe^2. Holdup dispersion arises from the presence of dead-end pores, and scales as *Pe* ln *Pe*. Each of these mechanisms will be manifest in the velocity fluctuation autocorrelation function, $\langle\boldsymbol{u}(0)\boldsymbol{u}(\tau)\rangle$, a measure of the correlation in fluid particle-velocity fluctuation over time τ.

Experimental Studies

We now present details of the apparatus employed in the experimental work reported here. Each NMR method employed is described successively in subsequent sections, and in each case the results of the method are discussed in the context of the related experimental data.

The NMR experiments were carried out using a Bruker AMX 300 NMR spectrometer based on a vertical wide-bore 7T magnet. The spectrometer was equipped with a flexible microimaging accessory, including a gradient coil set that incorporates three orthogonally directed gradients with amplitude up to 1.2 $\text{T}\cdot\text{m}^{-1}$. The sphere pack was composed of 90.7-μm-diameter monodisperse polymer spheres (Duke Scientific 7590A) compacted by centrifugation within a 1.9-mm-ID plastic tube. Deionized water was pumped through the sphere pack using a Pharmacia dual syringe pump at volumetric flow rates corresponding to seepage (tube) velocities within the range $0\le\langle v_{\text{tube}}\rangle\le 17.4\ \text{mm}\cdot\text{s}^{-1}$. The scaling between the interstitial pore and tube velocities is $\langle v\rangle=\langle v_{\text{tube}}\rangle/\phi$, where ϕ is the liquid volume fraction of the sphere pack. These flow rates correspond to Peclet numbers from 0 to 1,000. We follow Whitaker (Plumb and Whitaker, 1990; Quintard and Whitaker, 1993) in defining the Peclet number as

$$Pe=\frac{\langle v\rangle l}{D_0}=\left(\frac{\phi}{1-\phi}\right)\frac{\langle v\rangle d_p}{D_0}\approx\frac{\langle v_{\text{tube}}\rangle d_p}{D_{\text{eff}}}, \tag{4}$$

which incorporates a pore length scale $l=(\phi/(1-\phi))\,d_p$. The Peclet number takes on the simple form in the last equality in terms of the experimental parameters of the tube velocity, $\langle v_{\text{tube}}\rangle$, the particle diameter, d_p, and the effective restricted diffusion in the bead pack measured directly by NMR, $D_{\text{eff}}\approx(1-\phi)D_0$. Experimental Reynolds numbers based on the particle size and the calculated local interstitial velocity [$Re=(\langle v_{\text{tube}}\rangle/\phi)d_p/v$] in our work range from 0 to 4.

It is important to note that data from NMR experiments relate directly to the flow field of the liquid under investigation without the need to perturb the medium. The tracer particles are the fluid molecules themselves. This is in contrast to many other experiments found in the literature (Han et al., 1985) in which tracer particles are employed or where measurements are made of the concentration evolution of an injected solute interacting with the underlying solvent flow field. NMR, by comparison with all other techniques for the measurement of fluid translational motion, is quintessentially noninvasive.

Density and Velocity Distributions

The crucial distributions that may be said to characterize fluid in a porous medium are the fluid density, $\rho(\boldsymbol{r})$, and the local velocity $\boldsymbol{v}(\boldsymbol{r},t)$. If it were possible to gain complete information about $\rho(\boldsymbol{r})$ and $\boldsymbol{v}(\boldsymbol{r},t)$ over the entire domain of interest, then it could be said that both the morphology and hydrodynamics of the problem are completely known. On that basis we shall regard these two functions as fundamental to our theoretical framework.

In that context it is important to draw a distinction between Eulerian and Lagrangian formulations of $\boldsymbol{v}(\boldsymbol{r},t)$. It is the custom in fluid mechanics to adopt an Eulerian viewpoint (Koch and Brady, 1987) in which functions such as $\boldsymbol{v}(\boldsymbol{r},t)$ are space fixed rather than attached to a moving fluid element. In the latter case the relevant function would in fact be $\boldsymbol{v}(\boldsymbol{r}_0,\boldsymbol{r}(t))$, where $\boldsymbol{r}_0$ is coordinate of the relevant fluid element at the time origin. NMR is rather remarkable in that the signal originates from the spins contained in parent molecules swept along in the flow and generally detected without reference to individual locations, thereby engendering a fundamentally Lagrangian framework for the measurement of fluid parameters. There is one context, however, in which an element of traditional Eulerian perspective is overlaid, and that is the case of spatial imaging by means of laboratory-fixed magnetic-field gradients. In NMR imaging the volume elements (voxels) are locked in the fixed framework of the gradient coils, even though parameters associated with that voxel (for example, the local fluid velocity) are measured in a Lagrangian sense. It is important that this mixed perspective be appreciated. Indeed it is a consequence of this mixed perspective that the distinction between the Eulerian and Lagrangian character of the NMR measurement is quite subtle and image scale dependent when any spatial localization of the signal is implied.

Imaging of Density and Velocity

The imaging of fluid density by NMR is performed by spatial Fourier encoding using magnetic-field gradient pulses as shown in Figure 1a. The signal acquired is given by

$$S(\boldsymbol{k},0) = \int \rho(\boldsymbol{r}) \exp[i2\pi \boldsymbol{k}\cdot\boldsymbol{r}]\, d\boldsymbol{r}, \tag{5}$$

which on Fourier inversion yields

$$\rho(\boldsymbol{r}) = \int S(\boldsymbol{k},0) \exp[-i2\pi \boldsymbol{k}\cdot\boldsymbol{r}]\, d\boldsymbol{k}. \tag{6}$$

Imaging methodology is well established, and details can be found elsewhere (Callaghan, 1991). Figure 2 shows the spin density distribution, $\rho(\boldsymbol{r})$, image for the sphere pack. The resolution is (31.5 μm $\times$ 31.5 μm $\times$ 200 μm) per voxel (a volume element of the image comprising in this case a pixel of dimension 31.5 μm $\times$ 31.5 μm in a slice of thickness 200 μm).

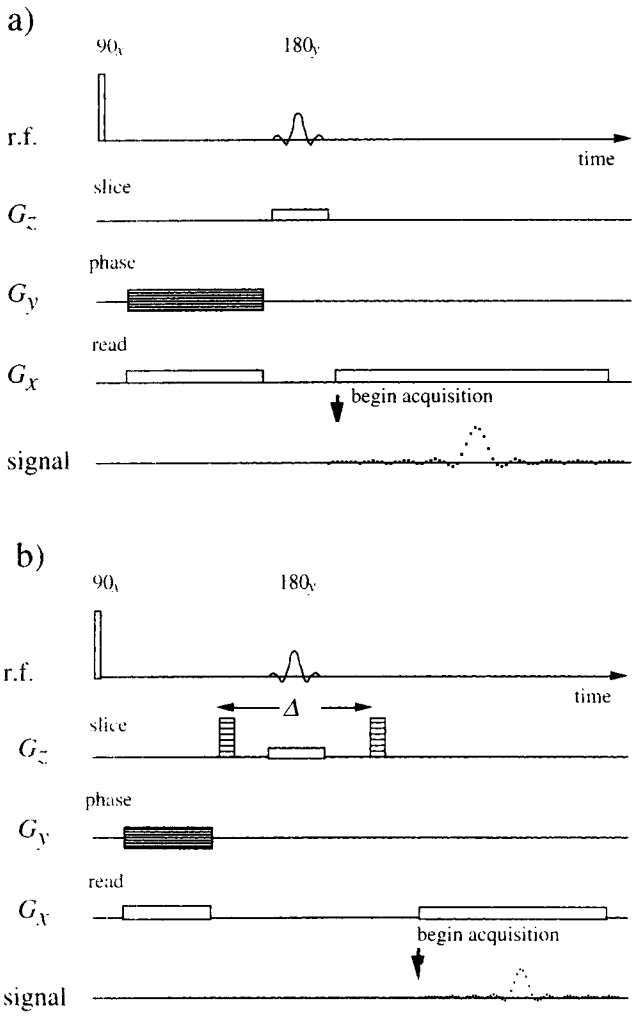

Figure 1. (a) Gradient and RF pulse sequence used for spin-echo Fourier imaging.

The initial (soft) RF pulse excites a rectangular layer of spins normal to the slice gradient (G_Z) axis; TE is the spin-echo time that occurs after the slice excitation: (b) gradient and RF pulse sequence for dynamic NMR imaging; the imaging gradients are preceded by a PGSE pulse pair to phase encode for motion.

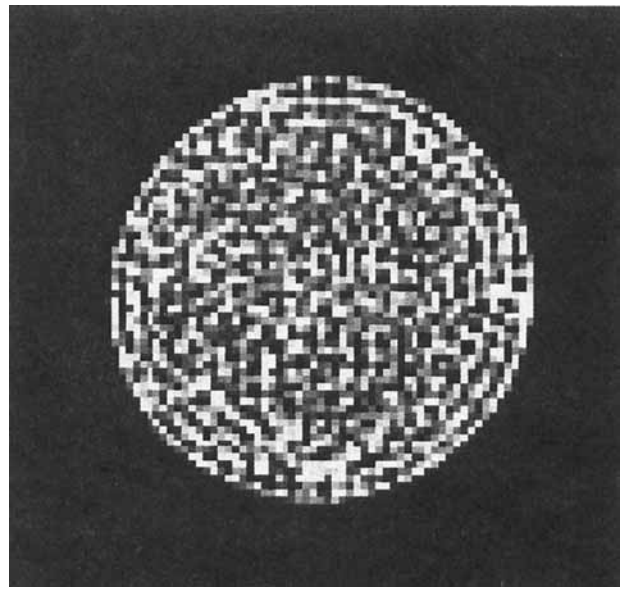

Figure 2. NMR image (128 $\times$ 128 pixel) of the ^{1}H spin-density distribution in the sphere pack.

High-intensity regions correspond to the water occupying pores between the spheres. The field of view is 4.0 mm and the slice thickness 200 μm.

Note the variation in packing across the sample, with a more ordered region near the tube wall, which results in variation in permeability across the sample. The measured spin density can be used in conjunction with a measurement on a pure-water reference to obtain the porosity (liquid volume fraction) of the sphere pack, $\phi = 0.44$.

A typical pulse sequence used for the imaging of flow is shown in Figure 1b. The signal acquired, $S(\boldsymbol{k},\boldsymbol{q})$, is modulated in the space of two wave vectors, $\boldsymbol{k} = (2\pi)^{-1}\gamma \boldsymbol{G}t$, which is conjugate to spin position, and $\boldsymbol{q} = (2\pi)^{-1}\gamma \boldsymbol{g}\delta$, which is conjugate to spin displacement over a fixed time Δ between the motion-encoding gradient pulses. In particular (Callaghan, 1991)

$$S(\boldsymbol{k},\boldsymbol{q}) = \int \rho(\boldsymbol{r}) \exp[i2\pi \boldsymbol{k}\cdot\boldsymbol{r}] \int P_S(\boldsymbol{r},0 \mid \boldsymbol{r}',\Delta) \times \exp[i2\pi \boldsymbol{q}\cdot(\boldsymbol{r}' - \boldsymbol{r})] d\boldsymbol{r}'\, d\boldsymbol{r}, \tag{7}$$

where $P_S(\boldsymbol{r},0 \mid \boldsymbol{r}',\Delta)$ represents the conditional probability that a spin residing at $\boldsymbol{r}$ at time 0 moves to $\boldsymbol{r}'$ at time t. Equation 7 can be rewritten

$$S(\boldsymbol{k},\boldsymbol{q}) = \int\int \rho(\boldsymbol{r}) P_S(\boldsymbol{r},0 \mid \boldsymbol{r}+\boldsymbol{R},\Delta) \exp[i2\pi \boldsymbol{k}\cdot\boldsymbol{r}] \times \exp[i2\pi \boldsymbol{q}\cdot\boldsymbol{R}]\, d\boldsymbol{R}\, d\boldsymbol{r}, \tag{8}$$

whereby inverse Fourier transformation yields

$$\rho(\boldsymbol{r}) P_S(\boldsymbol{r},0 \mid \boldsymbol{r}+\boldsymbol{R},\Delta) = \int\int S(\boldsymbol{k},\boldsymbol{q}) \exp[i2\pi \boldsymbol{k}\cdot\boldsymbol{r}] \times \exp[-i2\pi \boldsymbol{q}\cdot\boldsymbol{R}]\, d\boldsymbol{q}\, d\boldsymbol{k} \tag{9}$$

and

$$P_S(\boldsymbol{r},0 \mid \boldsymbol{r}+\boldsymbol{R},\Delta) = \frac{\int\int S(\boldsymbol{k},\boldsymbol{q}) \exp[-i2\pi \boldsymbol{k}\cdot\boldsymbol{r}] \exp[-i2\pi \boldsymbol{q}\cdot\boldsymbol{R}]\, d\boldsymbol{q}\, d\boldsymbol{k}}{\int S(\boldsymbol{k},0) \exp[-i2\pi \boldsymbol{k}\cdot\boldsymbol{r}]\, d\boldsymbol{k}} \quad (10)$$

Thus we can reconstruct the propagator that describes the motion of molecules spatially localized at $\boldsymbol{r}$ by the $\boldsymbol{k}$ gradient. Where a single $\boldsymbol{q}$-encoding direction is employed, it is customary to designate the component of $\boldsymbol{R}$ along $\boldsymbol{q}$ as

$$Z = \frac{\boldsymbol{R}\cdot\boldsymbol{q}}{q}, \quad (11)$$

where $q = |\boldsymbol{q}|$.

Inspection of $P_S(\boldsymbol{r},0 \mid \boldsymbol{r}+\boldsymbol{R},\Delta)$ enables us to calculate the mean displacement $\boldsymbol{R}_m$ for that voxel and hence the voxel mean velocity

$$\bar{\boldsymbol{v}}(\boldsymbol{r}) = \frac{\boldsymbol{R}_m}{\Delta}. \quad (12)$$

In interpreting $\bar{\boldsymbol{v}}(\boldsymbol{r})$ three important points need to be appreciated. First, the position encoding defines the coordinate $\boldsymbol{r}$ corresponding to the center of any voxel. We shall assume for simplicity that this encoding occurs at some specific instant of time, t_0, and emphasize this in the present argument by rewriting the voxel center coordinate as $\boldsymbol{r}_0$ while denoting the corresponding origin of any particular fluid element starting within the voxel by $\boldsymbol{r}'_0$. We shall then be required to take an average over all such elements. Second, we note that as a consequence, $\bar{\boldsymbol{v}}(\boldsymbol{r}_0)$ is both a temporal and spatial average. Note the use of the bar to represent a temporal averaging over a limited time range in contrast to the definition of $\boldsymbol{V}$ given earlier. The duration of the averaging time is on the order of T, the time required for spatial encoded data acquisition (Li et al., 1994), that is,

$$\bar{\boldsymbol{v}}(\boldsymbol{r}_0) = T^{-1}\int_0^T \langle \boldsymbol{v}(\boldsymbol{r}'_0,\boldsymbol{r}'(t))\rangle\, dt, \quad (13)$$

where T is typically on the order of minutes and $\boldsymbol{v}(\boldsymbol{r}'_0,\boldsymbol{r}'(t))$ is the Lagrangian velocity for fluid elements, starting within that voxel defined by the coordinate $\boldsymbol{r}_0$. Note that the spatial average indicated by the ensemble sum $\langle \ldots \rangle$ is over the voxel dimensions and has been presented in the weight function average formalism (Maneval et al., 1991; Quintard and Whitaker, 1993). Clearly, $\boldsymbol{r}_0 = \langle \boldsymbol{r}'_0 \rangle$.

Third, because $\boldsymbol{r}_0$ is frame-fixed, $P_S(\boldsymbol{r}_0,0 \mid \boldsymbol{r}_0+\boldsymbol{R},\Delta)$ is Eulerian in that sense. However we emphasize again that the encoding via $\boldsymbol{q}$ occurs in the frame of each spin over the time Δ and that both $\boldsymbol{R}_m$ and $\bar{\boldsymbol{v}}(\boldsymbol{r}_0)$ are determined by the history, over this period, of the Lagrangian function $\boldsymbol{v}[\boldsymbol{r}_0,\boldsymbol{r}(t)]$. For stationary (i.e., steady) flow, the Eulerian velocity associated with location $\boldsymbol{r}_0$ is constant. In that case the time duration of the integral in Eq. 13 could be reduced to Δ, the motion encoding time. Should the motion be unsteady, then the temporal average in Eq. 13 should indeed be taken over the entire image acquisition time, T. Thus, Eq. 13 as written allows for this more general case. In the sense that Δ may be taken to be sufficiently short as to provide a "snapshot" of the velocity over a time interval much shorter than T, we may to all intents and purposes regard $\boldsymbol{v}(\boldsymbol{r}_0)$ as Eulerian. Henceforth we drop the subscript and write this quantity simply as $\bar{\boldsymbol{v}}(\boldsymbol{r})$.

Notice that a knowledge of the voxel-averaged propagator $P_S(\boldsymbol{r},0 \mid \boldsymbol{r}+\boldsymbol{R},\Delta)$ enables a calculation of the variance in $\boldsymbol{R}$, a parameter that is directly related to the voxel-averaged dispersion coefficient. Thus the encoding method shown in Figure 1b allows not only a map of voxel-level mean velocity to be computed but also a map of mean dispersion at that scale.

Velocity images for flow in the sphere pack are shown in Figure 3. Figures 3a and 3b are mean-velocity maps for the tube velocities of 3.28 $\text{mm}\cdot\text{s}^{-1}$ and 6.55 $\text{mm}\cdot\text{s}^{-1}$, respectively (note the scale difference between the figures). In each case the spatial image resolution is $(63.5\text{-}\mu\text{m})^2$ pixel with 1,000-μm slice thickness, corresponding to a voxel volume of $(159\ \mu\text{m})^3$. The temporal resolution is $\Delta = 20$ ms for a single displacement phase-encoding step and $T \sim 60$ min for the entire data acquisition. The velocity images indicate significant positional variation in the mean velocity averaged over these space–time scales. Notice that all the velocity images indicate regions of higher velocity near the tube walls where the more ordered packing, evidenced in Figure 2, is present.

An intriguing feature is the difference in the spatial distributions for the two flow rates. The doubling of flow rate that occurs from Figures 3a to 3b appears to result in some spatial rearrangement of the regions of high and low velocity within the sample. Note that Mansfield and Issa (1996) have recently reported flow rearrangement at the same velocity for different initial conditions in rock using a rapid-velocity imaging technique, a phenomenon different to that observed here. Any interpretation of this apparent anomaly involves some subtlety in perspective. We emphasize again that the method of velocity measurement for each voxel is characterized by the averages shown in Eqs. 12 and 13. In the present work the slice thickness (the largest dimension of the voxel) encompasses many bead diameters. Furthermore, over the encoding time Δ, the fluid elements can move several pore spacings. Thus the nature of the temporal average is neither fine in the sense that a given starting voxel has a uniform fluid velocity, nor sufficiently coarse that the overall mean fluid velocity, $\langle v_{\text{tube}} \rangle/\phi$, is observed. The issue of graining size is clearly a delicate point in such measurements and is intricately tied to the spatial rearrangement observed. Further study of this phenomenon represents an important extension of this work.

Figure 3c is the mean velocity map for the flow rate in Figure 3a, 3.28 $\text{mm}\cdot\text{s}^{-1}$, obtained with a spatial resolution of $((95.2\ \mu\text{m})^2 \times 2{,}000\ \mu\text{m})$ per voxel and temporal resolution of $\Delta = 30$ ms and $T \sim 60$ min. The coarse graining (Kubo et al., 1991) in space and time that results from the increase in averaging scales tends to smooth the mean velocity data. This facility with NMR measurements to precisely control the averaging scales of the measurement provides a powerful means of investigating concepts such as the representative elementary volume (REV) (Bear, 1972; Quintard and Whitaker, 1993).

Quantitative velocity data taken from the images are shown in Figure 4. The average value of the velocities from the entire image data sets are given along the right ordinate. The coarse-grained image provides a mean velocity $\langle v_{\text{NMR}} \rangle = 7.44$

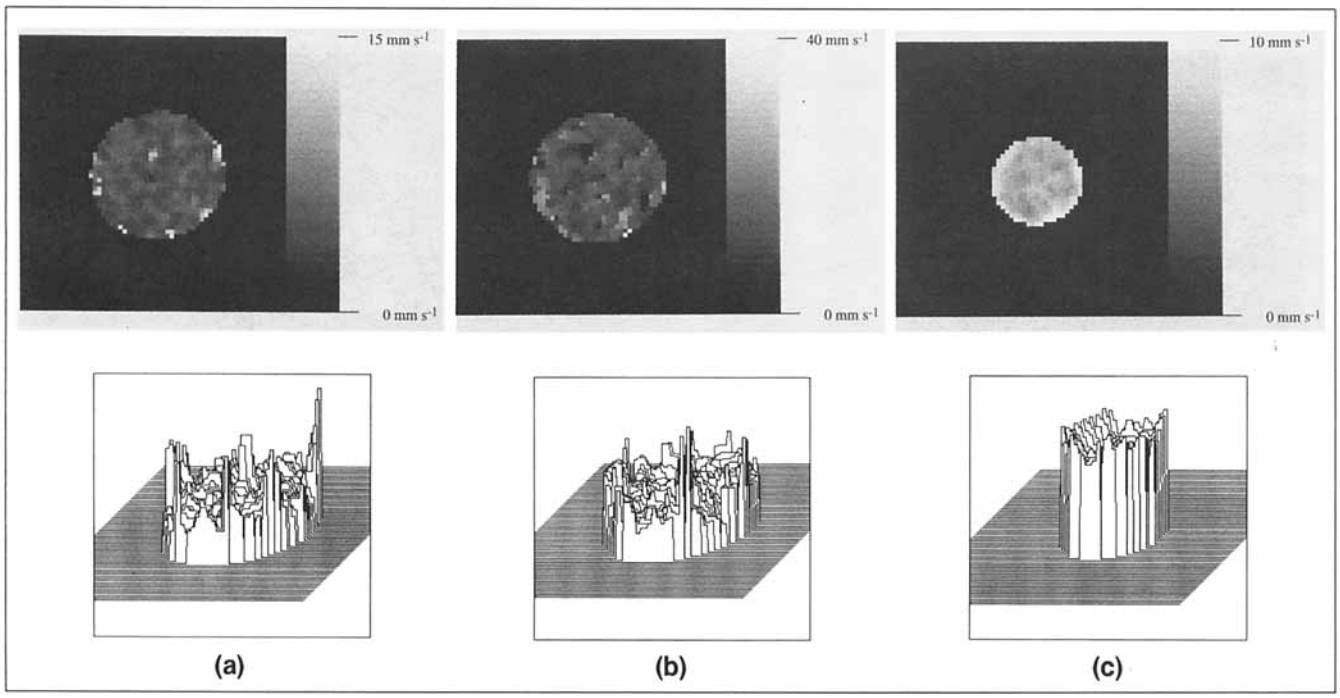

Figure 3. Grey-scale NMR images (64×64 pixels) and mesh plots of the spatial distribution of the mean velocity for tube velocities of (a) 3.28 mm·s^{-1} and (b) 6.55 mm·s^{-1}.

Note the scale difference between the figures. In (a) and (b) the spatial image resolution is (63.5 μm)^2 per pixel with a 1,000-μm slice thickness. In (c) the same flow rate as in (a) (3.28 mm·s^{-1}) is shown for a spatial resolution of (95.2 μm)^2 per pixel with a 2,000-μm slice thickness.

mm·s^{-1} in exact agreement with the scaling of the interstitial velocity in the porous media to the seepage velocity and porosity, $\langle v_{NMR} \rangle = \langle v_{tube} \rangle / \phi$. This indicates that in plane resolution of the order of the sphere diameter and slice thickness of 20 diameters provides data consistent with constant average-velocity scaling arguments. An important point is that multiplication of the higher-resolution data with the spin-density image will account for partial volume effects and close the mass balance. There are three regimes for spatially localized velocity images. Very-fine-resolution images, with few intravoxel boundaries and for which the local velocity is constant over the voxel, provide a measurement of the constant Eulerian-averaged velocity. Similarly, coarse-grained images, for which many pores are sampled, may also provide a constant Eulerian average. This coarse-graining character applies in the case of Figure 3c. It is in the intermediate regime, applicable in the data of Figures 3a and 3b, that great care in interpretation is required. In such circumstances the equivalence of Eqs. 12 and 13 may not hold and consequently anomalies may arise.

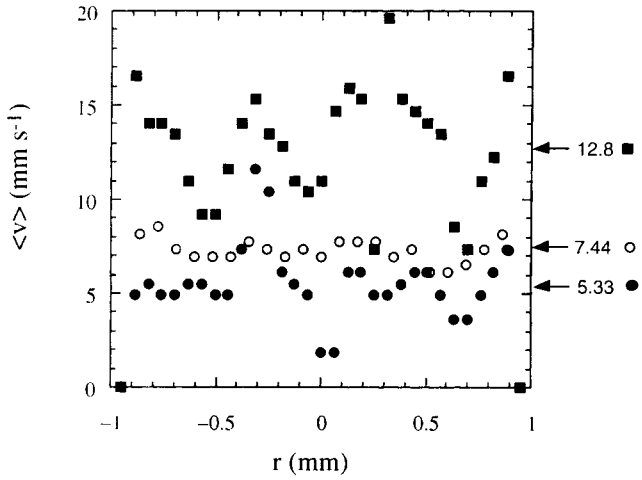

Figure 4. Quantitative radial velocity distributions obtained from a representative cross section of the image data of Figure 3.

The data correspond to mean tube velocities of Figure 3a (●) 3.28 mm^{-1}; 3b (■) 6.55 mm·s^{-1}; and 3c(○) 3.28 mm·s^{-1}. The mean velocities determined from the entire image are shown on the right.

By analyzing the spatial width of the propagator $P_S(\boldsymbol{r},0 \mid \boldsymbol{r} + \boldsymbol{R},\Delta)$ in each voxel, the variance in $\boldsymbol{R}$ can be computed, thus yielding an estimate of the voxel-averaged dispersion coefficient. Images of the voxel-averaged dispersion coefficients are displayed in Figures 5a and 5b for the flow rates and imaging parameters of Figures 3a and 3b, respectively. It is clear that not only does the mean velocity exhibit structural heterogeneity, but the dispersion also exhibits spatial variations associated with variations in the local structure and mean fluid velocity.

The spatial resolution available in NMR microscopy is, at best, around (20 μm)^3 and typically around (50 μm)^3. It is important to emphasize that the local propagator $P_S(\boldsymbol{r},0 \mid \boldsymbol{r} + \boldsymbol{R},\Delta)$ is consequently averaged over the voxel volume. Since localization comes at the price of increased averaging time, T, it is possible to reduce this duration down to the q-encoding time Δ, providing that spatial resolution is sacrificed.

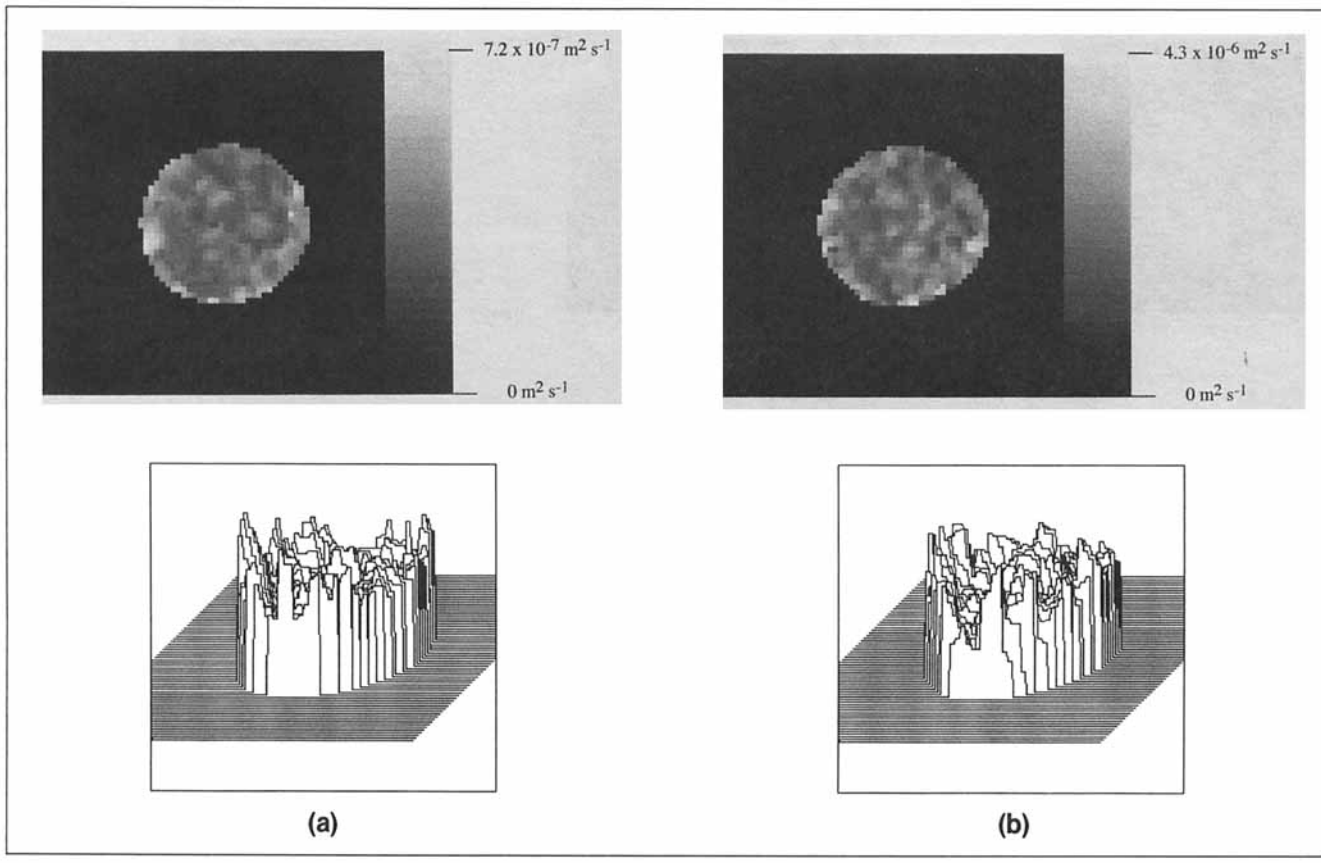

Figure 5. Grey-scale NMR images (64×64 pixels) and mesh plots of the spatial distribution of the mean dispersion for tube velocities of (a) 3.28 mm·s^{-1} and (b) 6.55 mm·s^{-1} (note the scale difference between the figures); the spatial image resolution is (63.5 μm)^2 per pixel with a 1,000-μm slice thickness as in Figures 3a and 3b.

PGSE NMR

Mean displacement via signal phase/average propagator analysis

Suppose that the spatial localization gradients are entirely omitted in a simple spin-echo experiment, as shown in Figure 6. The removal of spatial localization gradients returns us to purely Lagrangian encoding, and in all that follows parameters are Lagrangian. The echo attenuation is

$$E(\boldsymbol{q},\Delta) = \int\int \rho(\boldsymbol{r}) P_S(\boldsymbol{r},0 \mid \boldsymbol{r}+\boldsymbol{R},\Delta) \exp[i2\pi \boldsymbol{q}\cdot\boldsymbol{R}]\, d\boldsymbol{R}\, d\boldsymbol{r}. \tag{14}$$

By defining the average propagator (Karger and Heink, 1983) as

$$P(\boldsymbol{R},\Delta) = \int \rho(\boldsymbol{r}) P_S(\boldsymbol{r},0 \mid \boldsymbol{r}+\boldsymbol{R},\Delta)\, d\boldsymbol{r}, \tag{15}$$

one finds

$$E(\boldsymbol{q},\Delta) = \int P(\boldsymbol{R},\Delta) \exp[i2\pi \boldsymbol{q}\cdot\boldsymbol{R}]\, d\boldsymbol{R}. \tag{16}$$

Clearly $P(\boldsymbol{R},\Delta)$ represents an ensemble average over all spatial regions detected in the NMR experiment. Note the Lagrangian character of the propagator in which we follow the displacement history for the ensemble of individual fluid elements rather than individual volume elements.

The spatial resolution now depends on the sample size, for example, several (mm^3). However, it is now possible to encode for motion over a time Δ as short as 1 or 2 ms. Note that the averaged propagator can also be discussed in terms of the probability distribution for the averaged velocity (Garroway, 1974)

$$P(\boldsymbol{R},\Delta) = P(\bar{v}), \tag{17}$$

where $\bar{v} = \Delta^{-1}\int_0^\Delta \langle \boldsymbol{v}[\boldsymbol{r}_0,\boldsymbol{r}(t)]\rangle\, dt$, and the ensemble average is taken over all starting positions. Using the notation of Eq. 15 we can write

$$\bar{v} = \int d\boldsymbol{r}_0\, \rho(\boldsymbol{r}_0)\left\{\Delta^{-1}\int_0^\Delta \boldsymbol{v}(\boldsymbol{r}_0,\boldsymbol{r}(t))\, dt\right\}.$$

Hence we sacrifice spatial resolution but obtain the probability distribution of velocity averaged over a shorter time scale, typically 10 ms to 100 ms. Furthermore, we shall customarily utilize only one direction of displacement encoding gradient, $\boldsymbol{q}$, in any single experiment if we are to retain this temporal resolution. Consequently, the average propagator being measured should strictly be written, $P(Z,\Delta) = P(\bar{v})$.

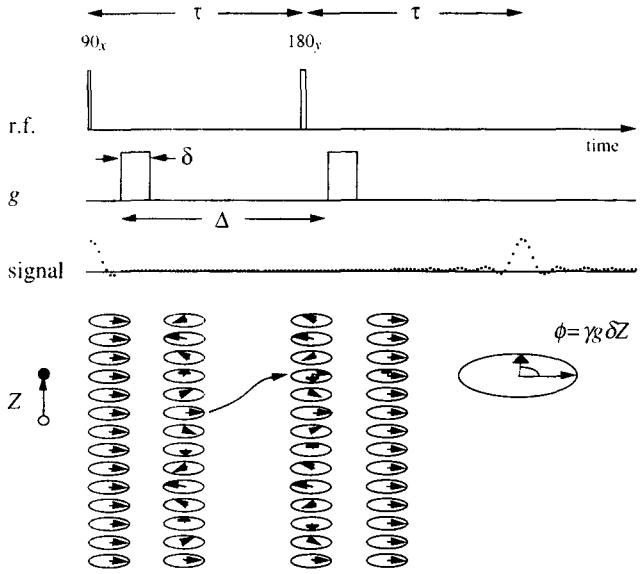

Figure 6. Gradient and RF pulse sequence for pulsed-gradient spin echo NMR. The gradient pulses have amplitude g, duration δ, and separation Δ.

Note that the first gradient pluse produces a helical phase twist in the transverse magnetization, along the gradient direction. This is unwound by the combination of a phase-inverting 180° RF pulse and a second gradient pulse. If molecules move along the gradient direction, the unwinding of the corresponding spin isochromat is incomplete and a residual phase shift, ϕ, results.

Averaged propagators for the flow in the sphere column are shown in Figures 7a–7c where the displacements, Z, are measured in the direction parallel to the mean flow. The spatial average is obtained over the tube cross section and the length of sample excited by the field of the radio frequency coil, $[\pi \times (0.95\ \text{mm})^2 \times 5\ \text{mm}]$. The data were obtained using 25 pulsed-gradient increments from 0 to 1.2 $\text{T}\cdot\text{m}^{-1}$, with the exact maximum chosen for each velocity so as to avoid signal aliasing. We point out, contrary to published misconceptions (Kutsovsky et al., 1996) that this experiment provides data on both positive and negative displacements owing to the Fourier relationship (Eqs. 8 and 9) between the average propagator, a real quantity, and the spin-echo signal, which is complex due to quadrature signal detection (Callaghan, 1991). Figure 7a displays the averaged propagators for a range of flow rates for $\Delta = 10$ ms. The data display the expected increase in displacement with increasing flow rate. Note that the propagator for no flow, $\langle v \rangle = 0$, is centered about zero displacement with a full width at half maximum proportional to the diffusivity. The diffusive width sets a resolution limit on the displacement that may be detected.

Kutsovsky et al. (1996) have recently reported the measurement of negative velocities for flow through sphere packs using this technique. For the flow studied here, no negative displacements are detected within the diffusion-limited experimental resolution. Figures 7b and 7c are plots of the averaged propagators as a function of the displacement time Δ for seepage velocities of 3.28 and 6.55 $\text{mm}\cdot\text{s}^{-1}$. The propagator maxima shift to larger displacements as Δ increases. The distributions of the displacements for the two flow rates

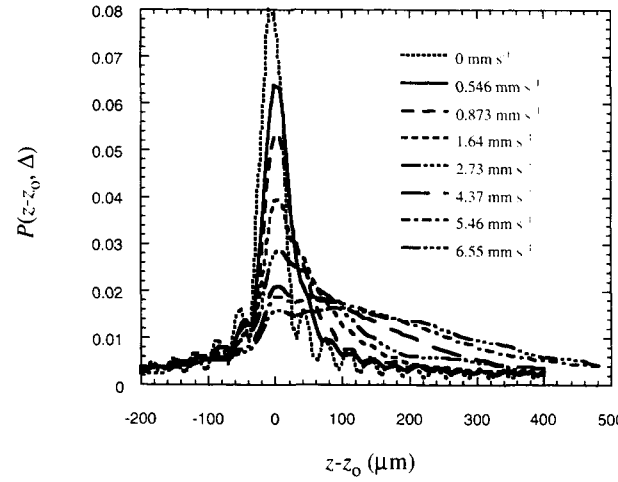

(a)

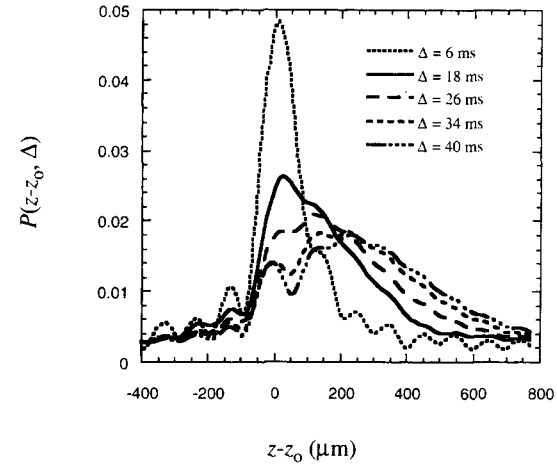

(b)

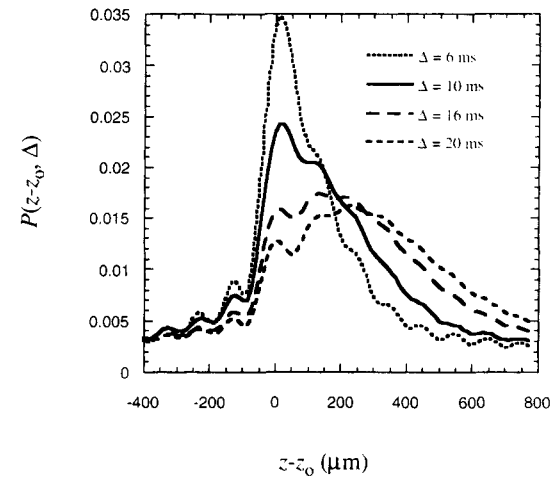

(c)

Figure 7. Averaged propagators, or displacement probability distributions, averaged over the entire sample.

In (a) propagators for several different flow rates at a fixed pulsed-gradient separation time of $\Delta = 10$ ms are shown. Propagators at two different tube velocities for a range of pulse-gradient separation times are shown in (b) 3.28 $\text{mm}\cdot\text{s}^{-1}$, and (c) 6.55 $\text{mm}\cdot\text{s}^{-1}$.

are quite similar. A pronounced peak persists at zero displacement, as was also reported by Barrall et al. (1994), indicating pronounced holdup effects due to molecules in regions of stagnation and the no-slip boundary condition at the sphere surfaces and tube wall. Several recent studies have dealt with detailed presentations of the average propagator over a range of times Δ using stimulated echo methods (Packer and Tessier, 1996; Lebon et al., 1996) as well as made comparison between the average propagator and spatially resolved velocity image data (Kutsovsky et al., 1996; Waggoner and Fukushima, 1996)

Displacement Fluctuations by Signal Modulus/ Correlation Function Analysis

Fluctuations in velocity field: dispersion

In the preceding section it was shown that the phase of the echo contained information from which the averaged velocity v could be calculated. We now address the issue of how the amplitude of the echo can be used to obtain information about temporal fluctuations in velocity. In general, spatial and temporal correlation functions of the Eulerian function $v(r,t')$ for general unsteady flow may be written as $\langle v(r,t)v(0,t)\rangle$ and $\langle v(r,t)v(r,0)\rangle$, respectively. For steady flow only the spatial fluctuation will be important for which the correlation function is simply $\langle v(r)v(0)\rangle$. However, when dealing with the fluctuating velocity distribution, in the Lagrangian sense of the PGSE NMR experiment, we are concerned only with the temporal Lagrangian correlation function averaged over all fluid elements. Furthermore, in dealing with this topic it is helpful to begin by using as a reference the ensemble-averaged mean velocity about which fluctuations may be said to occur. Again, allowing $\langle \ldots \rangle$ to represent a stationary ensemble average (either spatial averaging over a dimension much larger than the REV or temporal averaging over the longest fluctuation), we can write,

$$v_{ave} = \langle v(t) \rangle \tag{18}$$

$$v(t) = v_{ave} + u(t), \tag{19}$$

where $u(t)$ is the fluctuation velocity component with zero ensemble average. We note that $v(t)$, v_{ave}, and $u(t)$ are distributed over the sample space and are therefore functions of time only. In a strict sense, therefore, they may be contrasted with the *local* quantities v, V, and u discussed in the context of Eq. 1. Nonetheless, in the present context we can use Eq. 1 to define the averaged dispersion tensor in terms of correlations in $u(t)$.

We are concerned with the temporal correlation function $\langle u(t)u(0)\rangle$. From this ensemble average we can define the frequency-dependent dispersion tensor $D(\omega)$ as the Fourier spectrum of $\langle u(t)\, u(0)\rangle$ (Stepišnik, 1981), namely

$$D(\omega) = \int_0^\infty \langle u(t')u(0)\rangle \exp(i\omega t')\, dt'. \tag{20}$$

Generally, we make measurements using a single direction of gradient (e.g., along the z-axis), so that we are able to measure the component $D_{zz}(\omega)$. We term this scalar, the dispersion. Note that correlations of order higher than second have been neglected and a Gaussian assumption imposed.

The frequency-dependent dispersion tensor defined by Eq. 20 will have a spectral distribution dependent upon the characteristic correlation time for velocity fluctuations, τ_c. Using the symbol $u(t)$ to represent the component of the velocity fluctuation along the gradient (z-axis), the correlation time is defined by the relation

$$\tau_c = \langle u^2 \rangle^{-1} \int_0^\infty \langle u(t')u(0)\rangle\, dt'. \tag{21}$$

From this definition we derive the zero frequency amplitude of the dispersion coefficient,

$$D_{zz}(0) = \int_0^\infty \langle u(t')u(0)\rangle\, dt' = \langle u^2 \rangle \tau_c, \tag{22}$$

where τ_c is defined as the correlation time. This definition is exactly the form of the asymptotic dispersion coefficient (Eq. 1) from dispersion theory (Brenner, 1980; Brady, 1990; Van den Broeck, 1990).

Low q regime — the dispersion coefficient

PGSE NMR measurement yields an echo modulated both in amplitude and in phase by

$$E(q) = \exp(i2\pi q v_{ave})\, |E(q)|. \tag{23}$$

We have seen in the previous section how the phase-modulation term, $\exp(i2\pi q v_{ave})$, can be used to extract information about the mean velocity. Here we focus our attention on the amplitude modulation, $|E(q)|$. This variable can be extracted from the echo data either by "autophasing"(i.e., phase correcting the echo) or taking a modulus of the signal.

For the narrow pulse pair PGSE experiment shown in Figure 6, the weak gradient decay of the echo-attenuation function $|E(q)|$ may be written (Stepišnik, 1981; Callaghan and Stepišnik, 1996)

$$\lim_{q \to 0} -(4\pi^2\Delta)^{-1} \partial \log(|E(q)|)/\partial(q^2) \approx \exp(-4\pi^2 q^2 D^*\Delta), \tag{24}$$

where

$$D^* = \frac{\Delta}{\pi} \int_0^\infty D_{zz}(\omega) \operatorname{sinc}^2(\omega\Delta/2)\, d\omega. \tag{25}$$

Note that Eq. 24 is exact in the case that the distribution of fluid-element displacements is Gaussian. In general, however, the equation provides a working definition of the effective dispersion coefficient, D^*. This coefficient may depend on the observation time Δ in the case where Δ is comparable with or shorter than the correlation time τ_c. By contrast, when $\Delta \to \infty$, echo attenuation is sensitive to the zero frequency value of the dispersion spectrum and D^* assumes the asymptotic limiting value $D_{zz}(0)$.

The case of finite Δ may be handled analytically by assuming a simple expression for the correlation function $\langle u(t)u(0)\rangle$ such as the exponential, stationary Gaussian Markoff, form

$$\langle u(t)u(0)\rangle = \langle u^2\rangle \exp(-t/\tau_c). \tag{26}$$

This particular correlation function allows an exact analytic solution of Eq. 25 to yield

$$D^* = \langle u^2\rangle \tau_c[1+(\tau_c/\Delta)(\exp(-\Delta/\tau_c)-1)]. \tag{27}$$

The limits of this expression are

$$D^* = \frac{1}{2}\langle u^2\rangle \Delta \qquad \text{for } \Delta \ll \tau_c \tag{28}$$

$$= \langle u^2\rangle \tau_c \qquad \text{for } \Delta \gg \tau_c. \tag{29}$$

The effective dispersion coefficient, D^*, is thus obtained directly from the low-q limit of a plot of the spin-echo modulus as a function of the pulsed-gradient parameters, the Stejskal–Tanner plot (Stejskal and Tanner, 1965). The low-q limit is defined by the condition $4\pi^2q^2D^*\Delta \ll 1$. (In practice we restrict the exponent to less than or of order 0.3.) Stejskal–Tanner plots of representative echo-attenuation measurements at several flow rates, for the gradient oriented with the flow and a separation time $\Delta = 30$ ms, are displayed in Figure 8. The increase in the slope, that is, dispersion, of the low-q limit linear decay regime with increasing flow rate is clearly evident. Note that deviation from the Gaussian, or linear decay with q^2, behavior as q increases. We will return to this crucial aspect of the echo-attenuation behavior in due course.

The ability to vary the displacement encoding time Δ provides the means of determining the approach to asymptotic

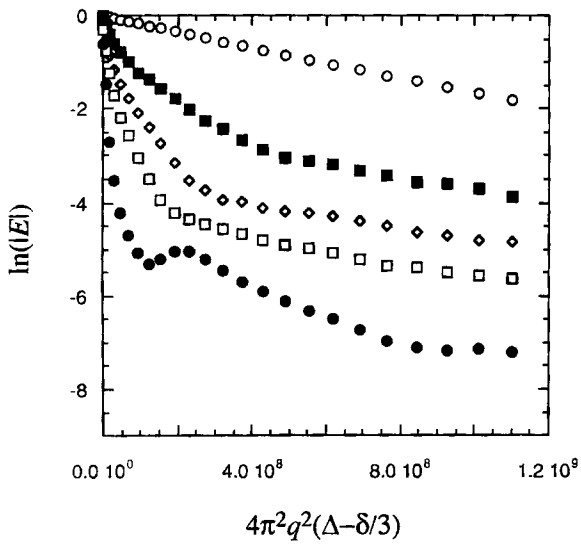

Figure 8. Stejskal–Tanner plot of the natural log of the modulus of the echo-attenuation function, E, as a function of the square of the wave vector.

The data are for tube velocities of (○) 0 mm·s^{-1}; (■) 0.546 mm·s^{-1}; (◇) 1.09 mm·s^{-1}; (□) 1.64 mm·s^{-1}; and (●) 3.28 mm·s^{-1}.

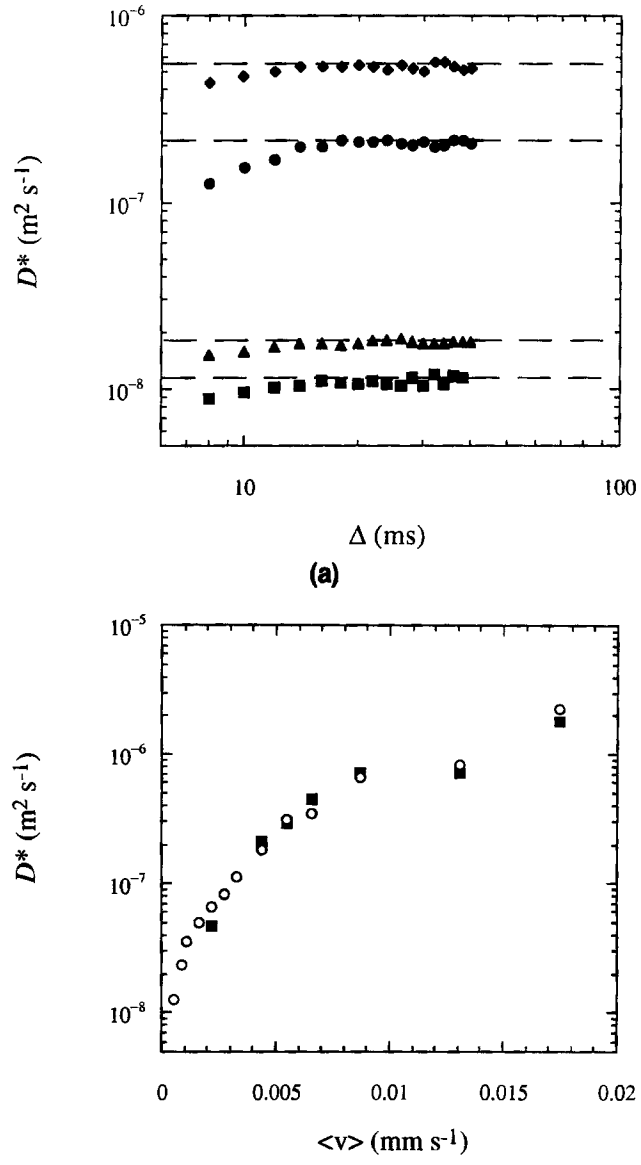

Figure 9. Dispersion coefficient or effective diffusivity as a function of: (a) displacement (gradient-separation) time for tube velocities of (■) 0.546, (▲) 1.09, (●) 3.28 and (♦) 6.55 mm·s^{-1}; (b) tube velocity for a single (○) and double (■) PGSE NMR experiment.

behavior of the dispersion coefficient and probe preasymptotic and anomalous time-dependent behavior (Koch and Brady, 1987; Brady, 1990). The time dependence of the dispersion coefficient, D^*, for four flow rates is shown in Figure 9a. These data indicate that the dispersion for the flow in the packed spheres is asymptotic, that is, time-independent, for times on the order of 16 ms or greater. Barrall (1995) has presented analogous results using the propagator to calculate positional variance. At first sight, this is in apparent conflict with rigorous scaling relations found in the literature (Han et al., 1985; Plumb and Whitaker, 1990) such as, $D_0t/l^2 \gg 0.3$, which for our system gives $t \gg 430$ ms. However, it is important to note that the scaling arguments are derived for a so-

lute that is introduced into the system at time $t = 0$, while the NMR experiments characterize the underlying fluid flow field without the need for a solute marker. The data show that the solvent flow field reaches an asymptotic state more rapidly than the scaling deduced from considerations based on a solute, in part because of the well-developed velocity distribution after an entrance length of $O(300d_p)$. PGSE NMR experiments that monitor both a solvent and a solute (Fischer et al., 1995) are a natural extension of the work presented here and will provide significant insight into the scaling questions raised.

An interesting feature of the limiting regimes $\Delta \ll \tau_c$ and $\Delta \gg \tau_c$ is that both lead to dispersion in the flow and both lead to echo attenuation in the PGSE NMR experiment. In one limit the dispersion coefficient is time-scale-dependent (Eq. 28), whereas in the other it is independent of the observation time, Δ (Eq. 29). An alternative test for the nature of the flow regime (Callaghan, 1991) is provided by the double PGSE sequence in which the sense of phase shift for displacements is opposite in the successive gradient pulse pairs. For the stationary flow field represented by the condition $\Delta \ll \tau_c$, the fluid element displacements will be identical for each pulse pair and the net phase spread across the ensemble following the second PGSE pair will be zero. For the regime $\Delta \gg \tau_c$ the displacements will be entirely uncorrelated and the variance in the phase spread will be doubled by the second pulse pair. In consequence a comparison of the echo attenuations for single and double PGSE pairs provides a powerful signature for temporal coherence. Comparison of the dispersion coefficient from double and single PGSE experiments using $\Delta = 10$ ms (Figure 9b) show complete agreement, as the data analysis accounts for a factor of 2 due to the second pulse pair. If by contrast the limit $\Delta \ll \tau_c$ applied, the double PGSE data would have a dispersion value equivalent to the molecular diffusivity alone, orders of magnitude smaller than the single PGSE data. The data of Figure 9b indicate that $\Delta \gg \tau_c$, in agreement with the results of the time-dependent measurements.

Asymptotic dispersion coefficient, D^*, in the limit $\Delta \to \infty$

In the asymptotic regime $\Delta \gg \tau_c$, D^* is independent of observation time Δ and well defined in a universal sense. The asymptotic dispersion coefficients obtained from the low-q limit of the NMR data for varying Peclet numbers are shown in Figures 10a–10c. Figure 10a presents the measured dispersion normalized by the water molecular diffusivity for displacement encoding times of $\Delta = 10$ ms and 30 ms. In agreement with the approach to the asymptotic limit exhibited in Figure 9a the preasymptotic dispersion data for $\Delta = 10$ ms is of smaller magnitude than that in the asymptotic regime at $\Delta = 30$ ms. The power-law scaling of the dispersion with the Peclet number, Pe^{α}, from a linear least-squares fit to the data yields a value of $\alpha = 1.37$ and a correlation coefficient, $r^2 = 0.984$, for both sets of data. Salles et al. (1993) discuss the Pe scaling, indicating regimes where the primary mixing mode in the flow is purely diffusive, $\alpha = 2$, purely mechanical, $\alpha = 1$, or due to regions of low and high velocity, $\alpha \sim 1.2$ ($D^*/D_0 \propto Pe \ln Pe$). The mixing in the flow studied here is thus of a complex nature due to multiple effects. We note that the power-law scaling found is close to the value of $\alpha = 1.34$ reported by Salles et al. (1993) for numerical simulations of reconstructed Fontainebleau sandstones with $\phi = 0.3$.

Longitudinal and transverse PGSE NMR dispersion data are plotted in Figures 10b and 10c, respectively, along with dispersion data collected from the literature (Han et al., 1985; Plumb and Whitaker, 1990, Quintard and Whitaker, 1993). The experimental conditions under which the non-NMR data were obtained is summarized in Han et al. (1985). Good agreement between the NMR data and data reported in the literature is evident. An important distinction should be drawn between the NMR data and that from concentration measuring techniques. PGSE NMR directly measures the displacement (velocity) correlation, and hence dispersion, as opposed to the indirect concentration-based methods that utilize solutions of the averaged advection-diffusion equation (Eq. 3) to calculate the dispersivity from the measured concentration and mean velocity data (Han et al., 1985). Finally, we note the particular utility of NMR in the ability to observe both longitudinal and transverse dispersivity by simple choice of magnetic-field gradient orientation.

Slow Temporal Correlations: Velocity Exchange (VEXSY) Spectroscopy

The measurement of dispersion by the attenuation in the spin-echo amplitude provides a means of gaining insight regarding fluctuations in the velocity over the time duration Δ between the gradient pulse pair. Let us now turn our attention to the partially averaged velocity, $\bar{v}$, and ask the question: Is it constant (and hence equal to $\langle v \rangle$) or do slow fluctuations remain on a time scale longer than Δ? As we discussed before in the context of the dispersive motion, the question as to whether motion is constant with time may be neatly addressed by an experiment in which the gradient pulse pairs are applied twice in succession.

We now examine a closely related NMR technique in which fluctuations in the mean velocity can be demonstrated in a very explicit manner. The relevant pulse sequence is shown in Figure 11. This experiment (Callaghan and Manz, 1994) is known as velocity-exchange spectroscopy (VEXSY) and returns a two-dimensional (2-D) spectrum in the space of two velocities $\bar{v}$ and $\bar{v}'$. This spectrum results from 2-D Fourier analysis of the signal with respect to the two independent displacement encodings. Given the ambiguities that can arise when the successive gradients have differing orientations it is customary to perform the experiment with a single gradient direction. Consequently we are concerned with the components of velocity, $\bar{v}$, along that direction.

While the phase encoding in one-dimensional PGSE NMR may be said to return the distribution $P(\bar{v})$, VEXSY measures conditional probability, $P_E(\bar{v} \mid \bar{v}', t)$ by the 2-D spectrum

$$S_t(\bar{v}, \bar{v}') = P(\bar{v}) P_E(\bar{v} \mid \bar{v}', t). \tag{30}$$

In effect it may be said that the VEXSY spectrum $S_t(\bar{v}, \bar{v}')$ allows us to calculate a very coarse-grained correlation function,

$$\langle \bar{v}(t)\bar{v}(0) \rangle = \int\int \bar{v}' \bar{v} P(\bar{v}) P_E(\bar{v} \mid \bar{v}', t)\, d\bar{v}'\, d\bar{v}$$
$$= \int\int \bar{v}' \bar{v} S_t(\bar{v}, \bar{v}')\, d\bar{v}'\, d\bar{v}. \tag{31}$$

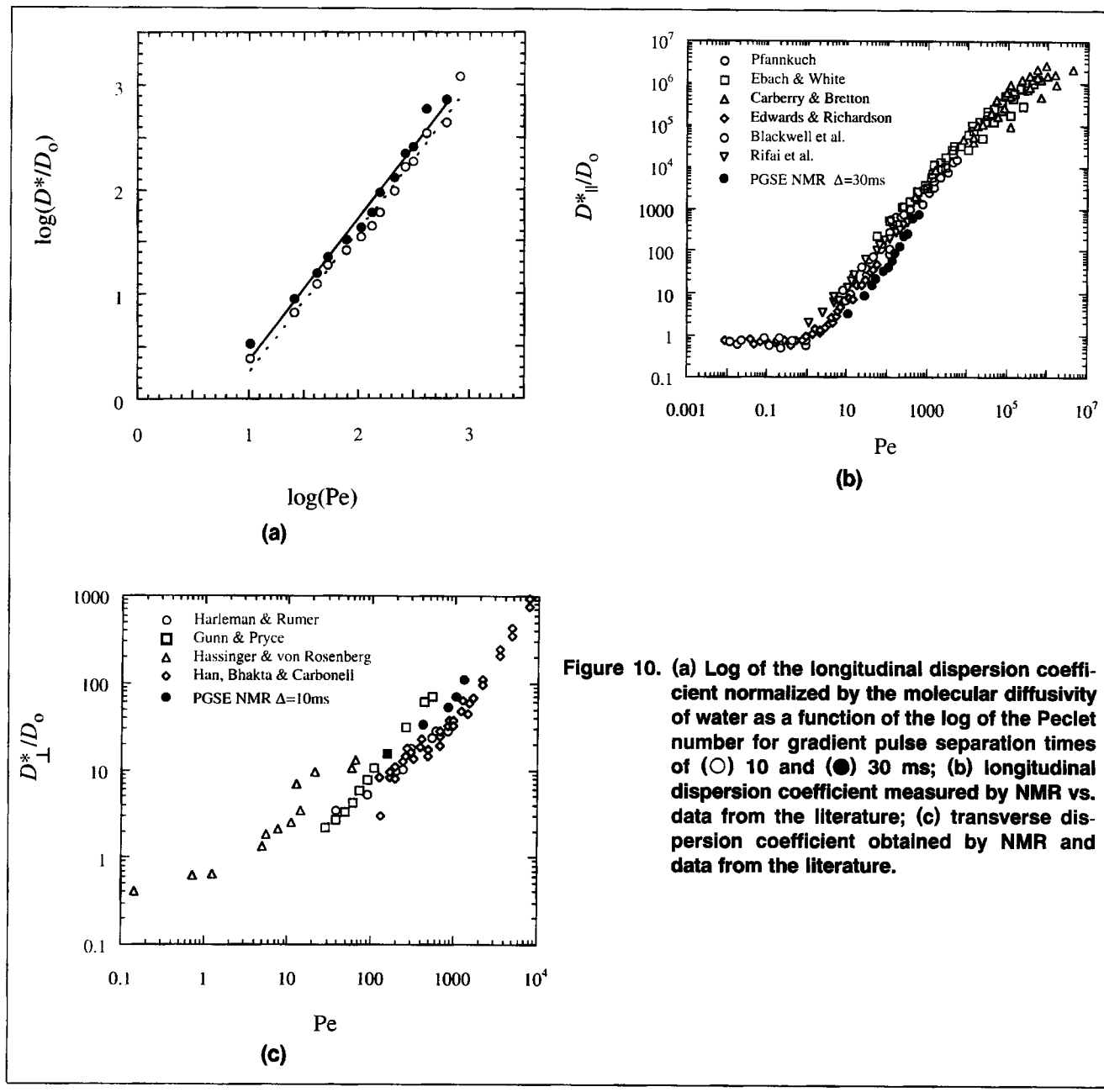

Figure 10. (a) Log of the longitudinal dispersion coefficient normalized by the molecular diffusivity of water as a function of the log of the Peclet number for gradient pulse separation times of (○) 10 and (●) 30 ms; (b) longitudinal dispersion coefficient measured by NMR vs. data from the literature; (c) transverse dispersion coefficient obtained by NMR and data from the literature.

Since, under directed flow, $\bar{v}$ has nonzero mean we note that the VEXSY spectrum will be displaced away from zero velocity and

$$\langle \bar{v}(t)\bar{v}(0)\rangle = \langle \bar{u}(t)\bar{u}(0)\rangle + v_{ave}^2. \tag{32}$$

Once again we stress that $P_E(\bar{v}\,|\,\bar{v}',t)$ is an ensemble average for common fluid elements and is therefore Lagrangian in character. It is a conditional velocity propagator, whereas $P_S(\boldsymbol{r},0\,|\,\boldsymbol{r}',t)$ was a conditional position propagator. However, it is also important to note that owing to the experimental limitations on the time t over which velocity changes can be observed using this method, the determination of $P_E(\bar{v}\,|\,\bar{v}',t)$ in the VEXSY experiment is confined to a rather coarse time resolution scale, t, greater than a few milliseconds at least. The utility of the experiment lies in our ability to test the stationarity of the mean velocity over this time scale. For example, if the velocity of each fluid element remains constant over the exchange time t, then the spectrum is confined entirely to the diagonal and $P_E(\bar{v}\,|\,\bar{v}',t)=\delta(\bar{v}-\bar{v}')$. The existence of off-diagonal features is thereby a signature for velocity fluctuations over time t. Equally if the velocities are fluctuating over the exchange time, but the distribution is perfectly stationary (i.e., its temporal fluctuations are asymptotic), then the shape of the spectrum, including its off-diagonal character, will not change as t is increased. Variations in spectral features indicate a nonstatic velocity distribution.

Figures 12a–12d are the VEXSY images of the mean velocity probability correlation. The displacement time scale over which the velocity mean is taken is $\Delta = 1$ ms. Figures 12a–12c are for a seepage velocity of $\langle v\rangle = 8.73\ \text{mm}\cdot\text{s}^{-1}$ and

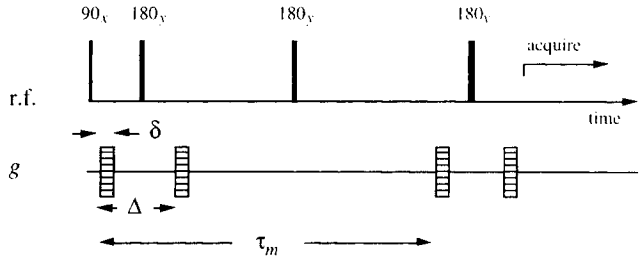

Figure 11. RF and gradient-pulse sequence for VEXSY in which successive PGSE pulse pairs (g_1 and g_2) are applied separated by a delay time τ_m.

velocity exchange times of $t_m = 5.2$ ms, 15.6 ms, and 52 ms. The images indicate that the shape of the spectrum does not change with t_m, implying that the temporal fluctuations in the mean velocity, averaged over a time scale of $\Delta = 1$ ms, are stationary over times greater than 5.2 ms. Figure 12d is for an exchange time of 4.8 ms at a velocity of 6.28 mm·s^{-1}, and the spectrum is of the same shape as for the higher velocity. This behavior stands in dramatic contrast to the dispersion data shown in Figure 9. The VEXSY experiment shows that fluctuations in the mean velocity reach asymptotic behavior at 5 ms, whereas the dispersion coefficient reaches its stationary asymptote at around 20 ms. This discrepancy suggests a distribution of time scales for the underlying dispersion processes and, in particular, the subtly different manner in which fluctuations in the mean velocity and the intrinsic dispersion are, respectively, influenced by that distribution arising from both mechanical and Taylor dispersion and

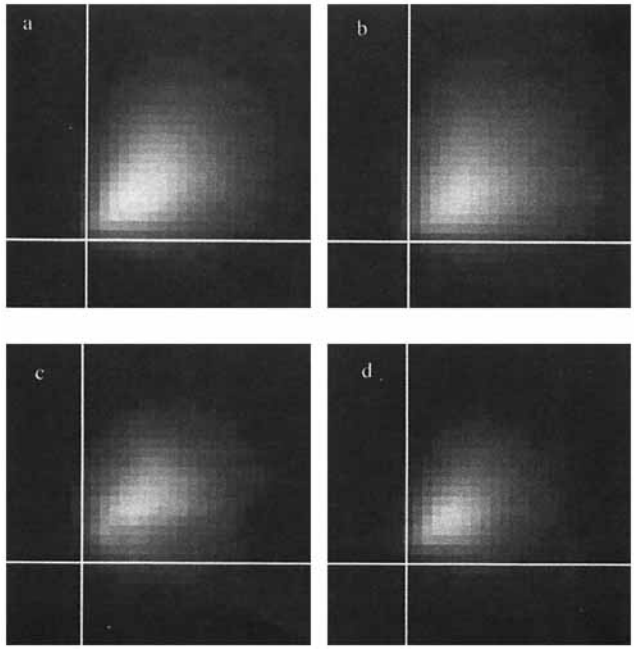

Figure 12. Succession of 2-D VEXSY images for water flowing through the bed of latex sphers.

τ_m corresponds to (a) 5.2 ms, (b) 15.6 ms, and (c) 52 ms for a seepage velocity of $\langle v \rangle = 8.73$ mm·s^{-1}, and (d) is for an exchange time of 4.8 ms at a velocity of 6.28 mm·s^{-1}. Note that the white lines indicate the zero displacement axes.

their associated macroscopic and molecular Brownian processes.

PGSE NMR Spatial Coherence and Flow Diffraction

Spatial correlation

Our description thus far is restricted to temporal correlations. Spatial correlation functions can, in principle, be obtained by judicious use of gradients that encode for position. At the simplest possible level, one could take the spatially resolved mean flow image shown in Figure 3 and calculate the function $\langle \bar{v}(\boldsymbol{r})\bar{v}(0)\rangle$ directly with a resolution of one imaging voxel. Given that one has already obtained a complete velocity map $\bar{v}(\boldsymbol{r})$ with that same resolution, it is clear that $\langle \bar{v}(\boldsymbol{r})\bar{v}(0)\rangle$ provides no additional information. The more interesting question concerns the analog to the nonspatially resolved PGSE NMR experiment. In that example spatial resolution was traded in favor of temporal resolution. One of the basic assumptions involved in averaging over the entire sample is that the REV of the porous medium is much smaller than the sample dimension. In other words, while the sample may be locally microscopically heterogeneous, over the macroscopic scale it is homogeneous. Hence the averaging process, from which one gains a signal-to-noise advantage, is representative of the structure.

A different type of experiment exists, in which spatial information is encoded in a manner that takes account of just this type of macroscopic averaging. It involves the acquisition of a signal from the entire sample under the imposition of a magnetic-field gradient. The repetitive, but nonperiodic, microscopic structure results in a diffraction pattern in $\boldsymbol{k}$-space where phase incoherence prevents NMR image reconstruction by direct Fourier inversion but, by Fourier inversion of the power spectrum, a spatial correlation function can be calculated (Barrall et al., 1992). Unfortunately this loss of phase information is fatal to the calculation of velocity by means of q-space encoding. Consequently, while the $\boldsymbol{k}$-diffraction method may be suitable for the calculation of density correlations, it is not amenable to the calculation of $\langle \bar{v}(\boldsymbol{r})\bar{v}(0)\rangle$.

PGSE NMR in the high-q regime: Flow diffraction

We now turn our attention to the PGSE NMR echo-attenuation experiment without the low-q restriction. We shall find that while this experiment is still sensitive to flow, it also yields unique information that is related to spatial correlations in the pore structure.

Equation 16 shows that the PGSE NMR experiment directly measures the Fourier spectrum of the displacement propagator $P(\boldsymbol{R},\Delta)$. In a porous medium $P(\boldsymbol{R},\Delta)$ will be characteristic both of the pore-space morphology and the flow-field characteristics, since the probability distribution of fluid element displacements will depend both on the existence of available pore space and on the hydrodynamic transport. In the absence of flow, Brownian motion transports molecules from site to site, and as a result, produces coherence effects in the wave-vector-dependant echo attenuation. This experiment has come to be known as "diffusive diffraction" (Callaghan et al., 1991; Callaghan, 1991; Callaghan et al., 1992).

The propagator resulting from diffusive transport of molecules within the pore structure is amenable to computation once the shape of pore boundaries is known. For example, in an orientationally disordered pore glass with pores of size a and spacing b, a pore-hopping formalism yields

$$E(q,\Delta) = |S_0(q)|^2 \times \exp\left[-\frac{6D_{\text{eff}}\Delta}{b^2+\xi^2}\left(1-\exp(-2\pi^2q^2\xi^2)\frac{\sin(2\pi qb)}{2\pi qb}\right)\right], \quad (33)$$

where $|S_0(q)|^2$ is the local pore factor; ξ is the pore spacing standard deviation; and D_{eff} is the diffusion coefficient for migration between pores. D_{eff} is measured in the low-q limit, long-range displacement region, and a coherence peak occurs at $q = b^{-1}$ (Callaghan et al., 1991; Callaghan et al., 1992; Coy and Callaghan, 1994). This model is predicated on the pore-equilibration assumption that the time scale for diffusive sampling of the pore is small relative to that for diffusion between pores, $a^2/D_0 \ll b^2/D_{\text{eff}}$.

Under conditions of flow the diffraction phenomenon is equally applicable (Seymour and Callaghan, 1996). Furthermore, the distance scale over which structural features can be probed is no longer restricted to the range of Brownian displacements over time Δ, but can be adjusted according to the flow rate. However, some subtle differences are apparent in flow diffraction, and these are nicely revealed in the experiments reported here. Whereas in diffusive diffraction the Brownian dynamics are everywhere similar except on the boundary layer, for flow the local hydrodynamics will strongly reflect the boundary conditions at all points in the pore space. For example, streamlines may be concentrated near a pore center, thus leading to greater probability of access but correspondingly shorter residency time. Thus the evolution times over which diffraction effects will be observed can be markedly different for differing regions of the pore structure.

A second major difference between flow diffraction and diffusive diffraction concerns the role of symmetry. Away from the boundary layer there is no favored direction for local displacements under Brownian motion. Under flow the symmetry is broken. As a consequence we might expect that diffraction effects observed when the scattering q-vector is aligned parallel to the flow will in general be different from those observed under transverse scattering.

The flow-diffraction phenomenon is clearly apparent in the echo-attenuation data for the sphere pack provided that the magnitude of q is no longer restricted to the range $4\pi^2q^2D^*\Delta \ll 1$. In the experiments reported here the effect of the mean flow is to produce a phase shift $\exp(i2\pi qv_{\text{ave}})$, while the dispersion results in a modulation in the echo amplitude. It is this latter term that contains all information about diffraction, and consequently we remove the phase shift and plot the magnitude of the echo amplitude, as in the previous analysis of dispersion under low-q conditions.

The deviation from Gaussian behavior seen in Figure 8 takes the form of coherences arising from diffraction effects. Figures 13a and 13b display echo attenuation for the longitudinal and transverse directions to the flow as a function of the reciprocal wave vector to displacement q. A prominent feature is the occurrence of the coherence peak in the transverse direction (Figure 13b) at a displacement reduced by nearly half relative to the displacement distance for the longitudinal coherence peak. This indicates the symmetry imposed by the flow and that it is the variation in the hydrodynamics that is probed by the flow diffraction effect, as opposed to only the media structure that is probed by the diffusive experiment (Callaghan et al., 1991, 1992; Coy and Callaghan, 1994) in which Brownian motion causes pore sampling. The coherence peak due to displacement correlation of nuclei manifests itself as velocity is increased. Increasing ve-

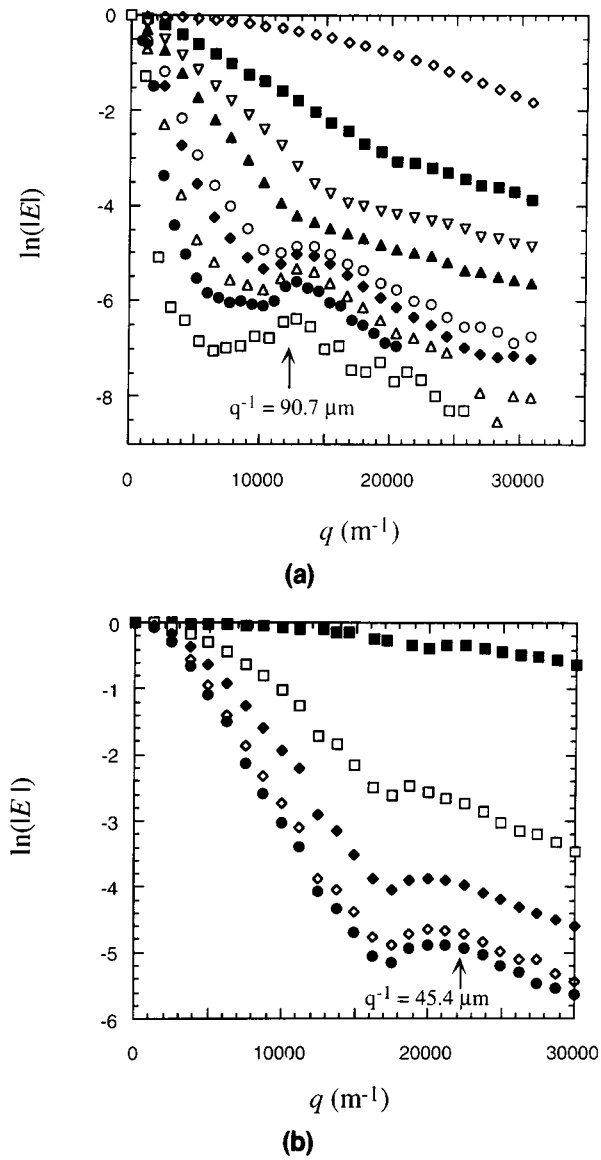

Figure 13. (a) Natural log of the modulus of the echo-attenuation function, E, as a function of wave vector for the gradient oriented in the longitudinal direction and $\Delta = 30$ ms.

The data are for tube velocities of (◇) 0 mm·s^{-1}, (■) 0.546 mm·s^{-1}, (▽) 1.09 mm·s^{-1}, (▲) 1.64 mm·s^{-1}, (○) 2.73 mm·s^{-1}, (◆) 3.28 mm·s^{-1}, (△) 4.37 mm·s^{-1}, (●) 5.46 mm·s^{-1}, and (□) 8.73 mm·s^{-1}. (b) As in (a) for the gradient oriented in the direction transverse to the flow with $\Delta = 10$ ms, at tube velocities of (■) 0 mm·s^{-1}, (□) 3.28 mm·s^{-1}, (◆) 8.73 mm·s^{-1}, (◇) 17.5 mm·s^{-1}, and (●) 21.8 mm·s^{-1}.

locity results in an increased length scale in the sampling of the pore spaces displaced from the starting pore. It is therefore equivalent to increasing the observation time, Δ, in an experiment without flow where only Brownian diffusion is available in the sampling of the pore spacing structure.

Figures 13a and 13b provide a visualization of the transition from Gaussian to non-Gaussian, and in a sense the local to nonlocal (Koch and Brady, 1987), dispersion behavior as the displacement scale decreases (q increases). The coherence peak indicates that the displacement of fluid particles is correlated over a displacement length scale of 83 μm, a value slightly reduced from the sphere diameter. Hence the velocity fluctuations may no longer be treated as Gaussian, and velocity fluctuation correlations of higher than second order must be retained in Eq. 20 and all subsequent developments. The direct relation between the flow-diffraction coherence phenomena and the nonlocal dispersion coefficient (Ding and Candela, 1996) is not transparent, as was the connection between the low-q PGSE NMR experiment and the dispersion coefficient in the asymptotic regime, since the nonlocal dispersion coefficient is expressed solely in terms of the second-order velocity-fluctuation correlation dependent on displacement and time step (Koch and Brady, 1987). Further investigation of these issues, potentially in the context of scattering theory (Frisch, 1968; Koch and Brady, 1987; Koch and Shaqfeh, 1992), which underlies the nonlocal development, should lead to further insight into both the NMR flow diffraction effect and nonlocal dispersion theory.

Conclusions

In this article we have illustrated how NMR experiments based on magnetic-field gradients can be used to study flow and dispersion in porous media in both the temporal and spatial domains. Because of the inherent insensitivity of NMR, it is necessary to employ a variety of approaches, each of which optimizes the parameters of interest, often by trading resolution in other physical variables. The dynamical basis of the various NMR methodologies has been presented in the context of well-established dispersion theory. It is clear from the results here that data obtained via the different experimental approaches can provide complementary information on transport phenomena at different spatial and temporal scales.

The choice of a packed bed of monodisperse spheres in which the size of the REV is close to the resolution limit of NMR imaging, helps to emphasize the importance of these complementary approaches. This limit, of around (100–1,000 μm)^3 implies the need for such generalized analysis in the case of most porous materials of practical interest. NMR velocity imaging has been shown to provide mean velocity and dispersion data over spatial scales on the order of the sphere diameter, but requires time averaging over the spatial encoding time. The data obtained are effectively Eulerian due to the long time average and spatial localization. By contrast, PGSE NMR without spatial encoding provides both mean velocity data via the phase shift in the signal, and mean dispersion information from the attenuation of the signal modulus, and over an averaging time that can be shorter by two orders of magnitude. This experiment, which is Lagrangian in perspective, involves an averaging over the entire sample dimensions, encompassing many REVs, and hence accessing directly the spatial ensemble average. The PGSE NMR method has been used to directly measure the asymptotic dispersion of theory, as well as the time- and spatial-dependence of the approach to asymptotic regimes. In this context the use of double PGSE pulse pairs and the methods of exchange spectroscopy can provide useful insight regarding stationarity and time dependence.

A remarkable aspect of the PGSE NMR method is the inherent coherence that leads to a formal analogy with scattering experiments. This coherence allows the experimenter to probe spatial and velocity correlations by a "scattering wave vector," thus gaining access to higher-order correlations, moments that are generally neglected in conventional dispersion theory based on limiting Gaussian behavior. We believe that the scattering approach has great potential in the study of complex flow properties involving the interplay between hydrodynamic and structural characteristics of the porous medium. Finally, we note that the techniques presented here are applicable to a wide class of media, including those that exhibit fractal scaling, thus providing a means for investigation of phenomena such as anomalous dispersion (Brady, 1990) in these more complex media.

Acknowledgments

This work was conducted while one of the authors (J.D.S.) was an NSF International Program Postdoctoral Fellow, grant INT-9500445. The authors thank Professor Steve Whitaker of UC Davis and his student Hicham el Mrini for providing the data used to generate Figures 10b and 10c. P.T.C. wishes to thank the New Zealand Foundation for Research, Science and Technology for funding support.

Literature Cited

Barrall, G. A., PhD Diss., Univ. of California, Berkeley (1995).

Barrall, G. A., L. Frydman, and G. C. Chingas, "NMR Diffraction and Spatial Statistics of Stationary Systems," *Science*, **255**, 714 (1992).

Barrall, G. A., Y. K. Lee, and G. C. Chingas, "Longitudinal and Transverse Displacement Distributions in Porous Flow," *Abstr. Experimental NMR Conf.*, p. 76 (1994).

Bear, J., *Dynamics of Fluids in Porous Media*, Elsevier, New York (1972).

Brady, J. F., "Dispersion in Heterogeneous Media," *Hydrodynamics of Dispersed Media*, J. P. Hulin, A. M. Cazabat, E. Guyon and F. Carmona, eds., Elsevier, New York (1990).

Brenner, H., "Dispersion Resulting from Flow Through Spatially Periodic Porous Media," *Philos. Trans. R. Soc. Lond. Ser. A*, **297**, 81 (1980).

Callaghan, P. T., *Principles of Nuclear Magnetic Resonance Microscopy*, Clarendon Press, Oxford (1991).

Callaghan, P. T., A. Coy, D. MacGowan, K. J. Packer, and F. O. Zelaya, "Diffraction-like Effects in NMR Diffusion Studies of Fluids in Porous Solids," *Nature*, **351**, 467 (1991).

Callaghan, P. T., A. Coy, T. P. J. Halpin, D. MacGowan, K. J. Packer, and F. O. Zelaya, "Diffusion in Porous Systems and the Influence of Pore Morphology in Pulsed Gradient Spin-Echo Nuclear Magnetic Resonance Studies," *J. Chem. Phys.*, **97**, 651 (1992).

Callaghan, P. T., and B. Manz, "Velocity Exchange Spectroscopy," *J. Mag. Res. A*, **106**, 260 (1994).

Callaghan, P. T., and J. Stepisnik, "Generalised Analysis of Motion Using Magnetic Field Gradients," *Adv. Opt. Magn. Reson.*, **19**, 325 (1996).

Chen, S. H., F. F. Qin, K. H. Kim, and A. T. Watson, "NMR Imaging of Multiphase Flow in Porous Media," *AIChE J.*, **39**, 925 (1993).

Coy, A., and P. T. Callaghan, "Pulsed Gradient Spin-Echo NMR 'Diffusive Diffraction' Experiments on Water Surrounding Close-Packed Polymer Spheres," *J. Coll. Int. Sci.*, **168**, 373 (1994).

Cushman, J. H., "An Introduction to Hierarchical Porous Media," *Dynamics of Fluids in Hierarchical Porous Media*, J. H. Cushman, ed., Academic Press, San Diego, CA (1990).
Dagan, G., *Flow and Transport in Porous Formations*, Springer-Verlag, Berlin (1989).
Davies, S., K. J. Packer, D. R. Roberts, and F. O. Zalaya, "Pore Size Distributions from NMR Spin-Lattice Relaxation Data," *Magn. Reson. Imaging*, **9**, 681 (1991).
Ding, A., and D. Candela, "Probing Non-Local Tracer Dispersion in Flows through Random Porous Media," *Phys. Rev. E*, **54**, 656 (1996).
Fischer, A. E., B. J. Balcom, E. J. Fordham, T. A. Carpenter, and L. D. Hall, "A Fast Inversion Recovery Method for Mapping Two-dimensional Tracer Diffusion and Dispersion in Heterogeneous Media," *J. Phys. D: Appl. Phys.*, **28**, 384 (1995).
Frisch, U., "Wave Propagation in Random Media," *Probablistic Methods in Applied Mathematics*, A. T. Bharucha-Reid, ed., Academic Press, New York (1968).
Garroway, A. N., "Velocity Measurements in Flowing Fluids by NMR," *J. Phys. D: Appl. Phys.*, **7**, L159 (1974).
Guilfoyle, D. N., P. Mansfield, and K. J. Packer, "Fluid Flow Measurement in Porous Media by Echo-Planar Imaging," *J. Magn. Reson.*, **97**, 342 (1992).
Han, N.-W., J. Bhakta, and R. G. Carbonell, "Longitudinal and Lateral Dispersion in Packed Beds: Effect of Column Length and Particle Size Distribution," *AIChE J.*, **31**, 277 (1985).
Karger, and Heink, "The Propagator Representation of Molecular Transport in Microporous Crystallites," *J. Magn. Reson.*, **51**, 1 (1983).
Koch, D. L., and J. F. Brady, "A Non-local Description of Advection-Diffusion with Application to Dispersion in Porous Media," *J. Fluid Mech.*, **180**, 387 (1987).
Koch, D. L., R. G. Cox, H. Brenner, and J. F. Brady, "The Effect of Order on Dispersion in Porous Media," *J. Fluid Mech.*, **200**, 173 (1989).
Koch, D. L., and E. S. G. Shaqfeh, "Averaged Equation and Diagrammatic Approximations to the Average Concentration of a Tracer Dispersed by a Gaussian Random Velocity Field," *Phys. Fluids A*, **4**, 887 (1992).
Kubo, R., M. Toda, and N. Hashitsume, *Statistical Physics: II. Nonequilibrium Statistical Mechanics*, Springer-Verlag, Berlin (1991).
Kutzovsky, Y. E., L. E. Scriven, H. T. Davis, and B. E. Hammer, "NMR Imaging of Velocity Profiles and Velocity Distributions in Bead Packs," *Phys. Fluids*, **8**, 863 (1996).
Lebon, L., L. Oger, J. Leblond, J. P. Hulin, N. S. Martys, and L. M. Schwartz, "Pulsed Gradient NMR Measurements and Numerical Simulation of Flow Velocity Distribution in Sphere Packings," *Phys. Fluids*, **8**, 293 (1996).
Li, T.-Q., J. D. Seymour, R. L. Powell, K. L. McCarthy, L. Odberg and M. J. McCarthy, "Turbulent Pipe Flow Studied by Time-Averaged NMR Imaging: Measurements of Velocity Profile and Turbulent Intensity," *Mag. Res. Imag.*, **12**, 923 (1994).
Maneval, J. E., M. J. McCarthy, and S. Whitaker, "Use of NMR as an Experimental Probe in Multiphase Systems: Determination of the Instrument Weight Function for Measurements of Liquid-Phase Volume Fractions," *Wat. Res. Res.*, **26**, 2807 (1990).
Mansfield, P., and B. Issa, "Fluid Transport in Porous Rocks I: EPI Studies and a Stochastic Model of Flow," *J. Mag. Res.*, **A122**, 137 (1996).
Mitra, P. P., P. N. Sen, and L. M. Schwartz, "Short-time Behavior of the Diffusion Coefficient as a Geometrical Probe of Porous Media," *Phys. Rev. B*, **47**, 8565 (1993).
Packer, K. J., and J. J. Tessier, "The Characterization of Fluid Transport in a Porous Solid by Pulsed Gradient Stimulated Echo NMR," *Mol. Phys.*, **87**, 267 (1996).
Plumb, O. A., and S. Whitaker, "Diffusion, Adsorption and Dispersion in Porous Media: Small Scale Averaging and Local Volume Averaging," *Dynamics of Fluids in Hierarchical Porous Media*, J. H. Cushman, ed., Academic Press, San Diego (1990).
Quintard, M., and S. Whitaker, "Transport in Ordered and Disordered Porous Media: Volume Averaged Equations, Closure Problems and Comparison with Experiment," *Chem. Eng. Sci.*, **48**, 2537 (1993).
Rubinstein, J., and R. Mauri, "Dispersion and Convection in Periodic Porous Media," *SIAM J. Appl. Math.*, **46**, 1018 (1986).
Salles, J., J. F. Thovert, R. Delannay, L. Prevors, J. L. Auriault, and P. M. Adler, "Taylor Dispersion in Porous Media. Determination of the Dispersion Tensor," *Phys. Fluids A*, **5**, 2348 (1993).
Sahimi, M., "Flow Phenomena in Rocks: From Continuum Models to Fractals, Percolation, Cellular Automata and Simulated Annealing," *Rev. Mod. Phys.*, **65**, 1393 (1993).
Seymour, J. D., and P. T. Callaghan, "Flow Diffraction' Structural Characterization and Measurement of Hydrodynamic Dispersion in Porous Media by PGSE NMR," *J. Magn. Reson.*, **A122**, 90 (1996).
Stepišnik, J., "Analysis of NMR Self-diffusion Measurements by a Density Matrix Calculation," *Physica B*, **104B**, 350 (1981).
Stejskal, E. O., and J. E. Tanner, "Spin Diffusion Measurements: Spin Echoes in the Presence of a Time Dependent Field Gradient," *J. Chem. Phys.*, **42**, 288 (1965).
Taylor, G. I., "Dispersion of Soluble Matter in Solvent Flowing Slowly Through a Tube," *Proc. R. Soc. Lond.*, **A219**, 186 (1953).
Van Den Broeck, C., "Taylor Dispersion Revisited," *Physica A*, **168**, 677 (1990).
Waggoner, R. A., and E. Fukushima, "Velocity Distribution of Slow Fluid Flows in Bentheimer Sandstone: An NMRI and Propagator Study," *Mag. Res. Imag.*, **14**, 1085 (1996).
Whitaker, S., "Multiphase Transport Phenomena: Matching Theory and Experiment," *Advances in Multiphase Flow and Related Problems*, G. Papanicolaou, ed., SIAM (1986).

Manuscript received Nov. 4, 1996, and revision received Mar. 26, 1997.